Simulated microgravity accelerates alpha-synuclein aggregation and induces oxidative stress in an *in vitro* Parkinson's disease model

#Lentini, Veronica[1]; #Uras, Giuseppe[1,2,4]; Manca, Alessia[1]; El Faqir, Mohammed Amine[1]; Lucas-Del-Pozo, Sara[2,4]; Deiana, Nicola[1]; Giacomo Cao[3]; Schapira, Anthony HV[2,4] & Pantaleo, Antonella[1].

1. Department of Biomedical Science, University of Sassari, Viale San Pietro, Sassari, 07100, Italy
2. Department of Clinical and Movement Neurosciences, UCL Queen Square Institute of Neurology, London, UK;
3. Department of Mechanical, Chemical and Materials Engineering, University of Cagliari, Piazza d'Armi, 09123 Cagliari, Italy
4. Aligning Science Across Parkinson's (ASAP) Collaborative Research Network, Chevy Chase, Maryland, USA

Corresponding authors

Prof. Anthony HV Schapira - a.schapira@ucl.ac.uk

Prof. Antonalla Pantaleo – apantaleo@uniss.it

Abstract

Parkinson's disease (PD) is a neurodegenerative disorder characterized by the accumulation of alpha-synuclein aggregates and progressive neuronal loss in the substantia nigra, with aging being its primary risk factor. The current available models to study PD mechanisms are largely relying on genetic mutations to recapitulate PD typical hallmarks, such as increased alpha-synuclein aggregation. However, they do not model the aging features associated with the disease.

Microgravity, a condition experience by astronauts during space missions, is known to induce ageing-like modifications on both systemic and cellular physiology.

To replicate the aging-related stress observed in PD patients, we exposed SH-SY5Y and 3K-SNCA mutant cell lines to simulated microgravity.

Our findings revealed that simulated microgravity enhanced PD alterations, with a significant increase in misfolded and phosphorylated a-syn. This was accompanied by heightened oxidative stress, as evidenced by increased levels of reactive oxygen species, without a sufficient antioxidant response. These results suggest that simulated microgravity effectively mimics and accelerate the stress associated with aging in PD cell models, regardless of the presence of PD mutation. This study

highlights the potential of simulated microgravity as a tool for investigating aging processes in neurodegenerative diseases.

Introduction

Parkinson disease (PD) is the second most common neurodegenerative disorder and is characterized by both motor and non-motor clinical features [1–3]. PD is defined pathologically by the presence of alpha-synuclein (a-syn) aggregates in Lewy Bodies and neurites with associated loss of pigmented dopaminergic neurons in the substantia nigra parts compacta (SNc). A-syn is a member of a group of intrinsically disordered amyloid proteins that assemble into oligomeric and fibrillar aggregates [4–8].

The exact aetiology of PD is still unknown. The most important risk factor for developing PD is advancing age. Variants in genes like *SNCA, GBA1, PINK1, PRKN, and LRRK2*, contribute to the disease pathology, of which the most important risk factor are the mutations in the *GBA1* gene, found in 10-15% of PD patients [9–15]. *GBA1* is located on chromosome 1 and encodes the lysosomal hydrolase glucocerebrosidase (GCase, or acid-β-glucosidase) that catalyses the cleavage of glucosylceramide (GlcCer) and glucosylsphingosine (GlcSph) into glucose and ceramide, or glucose and sphingosine, respectively [16].

A-syn toxic accumulation has been associated with impairment in several cellular functions, involving mitochondria, proteasomes and lysosome, as well as endoplasmic reticulum (ER) stress, axonal transport deficiencies and, ultimately, impaired dopamine synaptic release [17].

Additionally, a-syn oligomers trigger apoptotic pathways via reactive oxygen species (ROS) production [18,19].

The lysosome plays a critical role in the clearance of a-syn; it is physiologically degraded by both the ubiquitin-proteasome system and the autophagy lysosomal pathway (ALP), using mainly chaperone-mediated autophagy (CMA) and macroautophagy [20–24]. Moreover, lysosomal proteins which are crucial for both macroautophagy and CMA and have been found to be defective in the post-mortem brains of PD patients [25]. Patients with *GBA1* mutations exhibit decreased lysosomal GCase enzyme activity in multiple brain regions [26]. Impairment of GCase activity leads to lysosomal dysfunction, obstructing the trafficking and processing of a-syn [27,28]. Conversely, lysosomal dysfunction can be induced by a-syn itself [29], mainly by interrupting the transport of lysosomal hydrolases from the ER to the Golgi apparatus and the lysosome in neurons [30–32]. Consequently, overexpression of a-syn reduces both GCase activity and protein levels, resulting in a reciprocal biochemical connection between a-synuclein and GCase [33–36].

A-syn accumulation can induce ER stress by disrupting protein trafficking and directly interacting with ER membranes. In addition, ER stress exacerbates a-syn toxicity, forming a feedback loop that contributes to neurodegeneration in synucleinopathies [37–39].

In addition to this, a-syn aberrant accumulation has been linked to increased oxidative stress, a cellular status characterized by an accumulation of ROS. The latter is defined by an imbalance in ROS production and the ability of the cell to increase its antioxidant response, causing cellular toxicity at multiple levels, ranging from altered mitochondrial function to membrane damage.

Microgravity, the condition that is naturally experienced by astronauts in space, has been shown to induce oxidative stress by increasing ROS productions and lipid peroxidation. Space agencies such as the National Aeronautics and Space Administration (NASA) and the European Space Agency (ESA) conduct experiments aboard space stations like the International Space Station (ISS) to explore phenomena not observable under terrestrial gravity (1g). Microgravity profoundly affects biological

systems, from single cells to entire organisms and cellular adjustment in these conditions can help the exploration of diverse pathophysiological processes [40–48].

Simulated microgravity (s-μg) environment also impairs cellular stress responses, including the unfolded protein response and protein turnover, which may, in turn, lead to the accumulation of misfolded protein.

These findings imply a potential induction of senescence across various cellular models, including cancer cell lines, stem cells, and differentiated cells [49–52]. While further investigation is necessary to fully understand the implications of microgravity on senescence, several researchers propose that exposure to microgravity triggers cellular aging, possibly through heightened oxidative stress resulting from mitochondrial dysfunction [44,53–58]. This process may initiate apoptotic pathways and alter cellular proliferation, differentiation, and growth [51,59].

In the present study, a systematic characterization of PD features under s-μg conditions using a random positioning machine (RPM) was performed, focusing on a-syn alterations, including the formation of aggregates, lysosomal physiology, and oxidative stress. We employed two neuronal cell line models, the SH-SY5Y and a-syn mutant 3K-SNCA line. Whilst the first cell line is widely used as a model for neurodegenerative disorders [60,61], the mutant line is designed to accelerate a-syn aggregation. Specifically, the familial PD-linked mutation E46K, which changes the a-syn repeat motif KTKEGV to KTKKGV in repeat 4, was amplified by inserting analogous mutations into the immediately adjacent KTKEGV repeat motifs (E35K+E46K+E61K), stabilizing membrane-associated helical a-syn, hence promoting the protein oligomerization and eventual aggregation [62,63].

Our study shows that s-μg conditions result in a-syn alterations and oxidative stress in mutated and wild type cells, indicating that s-μg exposure leads to increased a-syn accumulation and aggregation, independently of the presence of a-syn mutations.

Methods

Cell culture

Human neuroblastoma cells SH-SY5Y (ATCC number: CRL-2266) and 3K-SNCA cells were cultured in DMEM/F-12, GlutaMAX™ medium (10565018; Gibco) supplemented with 10% fetal bovine serum (FBS) and 1x Penicillin/Streptomycin (Pen/Strep) at 37° C and 5% CO_2 in T-75 flasks.

Microgravity

The Random Positioning Machine (RPM) was used as a microgravity simulator, while, although it cannot be directly compared to the real condition of microgravity, it still serves as a valuable tool for conducting preliminary tests [64]. It is composed by two frames that rotate independently. The samples, which are placed close to the centre in the inner frame, are subjected to a mean gravity force close to zero g, due to the continuous re-orientations and random movements of the axes.

The flasks containing the cells were carefully filled up with complete medium to avoid the shear forces and to allow the cells to maintain a state of free-fall motion. For the experiment, the Random Walk mode was used with a velocity of 60 deg/sec. Cells were left in the machine for different time points (24 hours and 48 hours) and compared with the 1g control group placed in the static bar of the RPM.

Bradford Assay

Bradford assay was used as a method to quantify the concentration of proteins in samples using bovine serum albumin as a standard according to manufacturer instruction (B6916; Sigma Aldrich).

124 ***Western Blot Analysis***

125 Cells pellets were lysed, and proteins were separated as previously described [65]. The primary
126 antibody were added at the following concentrations: rabbit anti a-syn 1:1000 (ab138501; abcam);
127 mouse anti-GBA1 1:500 (AP1140; Calbio Biochem); mouse anti β-Actin 1:10000 (ab6276; abcam);
128 mouse anti LAMP1 1:500 (611042; BD Trasduction), mouse anti p-Synuclein (Ser129) 1:1000
129 (ab51253; abcam), rabbit anti Catalase 1:1000 (ab209211; abcam), and mouse anti ATF6 1:500
130 (ab227830; abcam). The secondary antibody was added at a 1:2000 final concentration: Goat anti-
131 mouse HRP (P0447; Dako) and goat anti-rabbit HRP (P0448; Dako). The membrane was imaged prior
132 incubation with ECL reagent using the ChemiDoc Imaging System.

133

134 ***Immunostaining and Confocal***

135 Immunostaining was performed as previously described [60,66]. The primary antibodies were added
136 at the following concentrations: mouse anti a-syn antibody 1:750 (SIG-39730; BioLegend) and rabbit
137 anti-LAMP1 1:2000 (ab278043; abcam). The secondary antibodies were added at the following
138 concentrations: 1:2500 Goat anti-Rabbit IgG (H+L) Highly Cross-Adsorbed Secondary Antibody, Alexa
139 Fluor™ Plus 647 (A32733; Invitrogen) and 1:2500 Goat anti-Mouse IgG (H+L) Highly Cross-Adsorbed
140 Secondary Antibody, Alexa Fluor™ Plus 488 (A32723; Invitrogen). 1ng/ml of Hoechst solution (62249;
141 Thermo Scientific) was used to visualize the nuclei. The slides were imaged using the Nikon C2
142 Confocal Microscope.

143

144 ***ROS quantification***

145 ROS levels were quantified using Invitrogen™ carboxy-H2DCFDA (C400; Invitrogen) as a fluorescent
146 indicator with a final concentration of 20µM. The experiment was performed on live cells which

147 were prepared by adding 0.5µl of protease inhibitor and anti-phosphatase 1 and 2 to the cell pellets.
148 1µl of pellet was diluted in 1ml of PBS. H_2O_2 was used to prepare a standard curve for different ROS
149 concentrations, using PBS as a control for 0µM ROS. 100 µl of diluted samples and standards were
150 added to a black 96-well plate with 92µl PBS and 8µl carboxy-H2DCFDA probe. After a 1hour
151 incubation in the dark at 37°C with 5% CO_2, using a filter-based reader (fluorescence), samples were
152 analysed with an excitation of 488nm and emission of 530nm. Final values were normalised for the
153 total amount of protein, quantified using the Bradford assay.
154
155 ***MDA quantification***
156 The Cayman TBARS assay kit (10009055; Cayman) was performed to measure Malondialdehyde
157 (MDA) levels. In this kit, MDA and Thiobarbituric Acid (TBA) react under high temperature (90-100°C)
158 and acidic conditions, and their product is measured colorimetrically at 530-540nm. MDA standard
159 was diluted to create a stock solution of 125µM, and a standard curve was prepared with varying
160 MDA concentrations. Samples and standards were added to Eppendorf® tubes, along with the SDS
161 solution and the Color reagent (composed of Thiobarbituric Acid, Acetic Acid, and NaOH) according
162 to the manufacturer instructions. The mixture was heated for 1 hour at 100°C, cooled on ice for 10
163 minutes, centrifuged for 10 minutes at 1,600 x g at 4°C, and then loaded in a clear plate for
164 absorbance reading at 530-540 nm. The standard curve was plotted, and unknown values were
165 interpolated after subtracting the blank. Final values were normalised for the total amount of
166 proteins, quantified using the Bradford assay.
167
168 ***Total Antioxidant Capacity (TAC) quantification***
169 Cayman's Antioxidant Assay (709001, Cayman) is a versatile method for assessing the total
170 antioxidant capacity (TAC) of various biological samples. This assay evaluates the combined

171 antioxidant activities of a range of constituents, such as vitamins, proteins, lipids, glutathione, and
172 uric acid.

173 All the reagents and samples were prepared and diluted according to manufacturer instructions.

174 Trolox standard wells received 10µl of Trolox standard (from a concentration of 0µM to 0.33 µM as
175 suggested in the assay protocol), 10µl of metmyoglobin, and 150µl of chromogen per well. Similarly,
176 sample wells were prepared with 10µl of sample, 10µl of metmyoglobin, and 150µl of chromogen.
177 The reactions were initiated by adding 40µl of hydrogen peroxide working solution to all the wells.
178 It is crucial to add the hydrogen peroxide quickly (within one minute is recommended when using a
179 multichannel) to ensure uniform reaction initiation across wells. The plate was then covered and
180 incubated on a shaker for five minutes at room temperature to allow for the completion of the
181 reactions. After incubation, the plate cover was removed, and the absorbance was measured at 405
182 nm using a plate reader. The standard curve was plotted, and unknown values were interpolated
183 after subtracting the blank, values were then multiplied for the dilution factor. Final values were
184 normalised for the total amount of proteins, quantified using the Bradford assay.

185

186 ***DATA analysis***

187 Statistical comparisons and analysis were performed using GraphPad Prism 9.1 software. The
188 Shapiro-Wilk test was first used to determine whether the collected data was normally distributed.
189 In non-normally distributed data, Kruskal-Wallis test and Dunn's post-hoc analysis were used to
190 conduct multiple comparisons. The differences between three or more groups of normally
191 distributed samples were compared using the ANOVA test. Each experiment was conducted three
192 times. Each condition was carried out in triplicate in every experiment conducted. Results are

193 displayed as mean ± standard error of the mean. Results were considered statistically significant if
194 their p-value was less than 0.05.

195

196 **Results**

197 ***A-syn pathogenic species are modulated by s-μg exposure***

198 To study whether s-μg exposure influences a-syn protein behaviour, we quantified various species
199 of the protein. Initially, we questioned whether the total level of a-syn is affected by prolonged
200 exposure to s-μg. Thus, two different time points (24 and 48 hours) were assessed to monitor the
201 changes in a-syn levels. We then studied whether a change in total levels of a-syn would translate in
202 the different subspecies of the protein. We quantified aggregated forms of a-syn which are known
203 to impair lysosomal function, induce ER stress, and promote an aberrant UPR [26,67,68].

204 The initial investigation on total a-syn levels, using a western blot approach, did not reveal any
205 significant difference between cells exposed s-μg and those cultured in 1g, independently of the
206 SNCA mutation (Fig. 1 a-d). These findings suggest that the overall quantity of a-syn in cell cultures
207 in s-μg is not affected. However, confocal microscopy analysis of 3K-SNCA cells exposed to s-μg
208 revealed a significant increase in a-syn aggregates after just 24 hours of exposure (P=0.0007), with a
209 further marked increase following 48 hours of incubation in the s-μg gravity environment
210 (P=0.000006) (Fig. 2 a, b). To ensure that the observed effects were not due to a combined influence
211 of the 3K mutation and s-μg, we exposed the SH-SY5Y control cell line to s-μg. This experiment
212 revealed a significant increase in a-syn aggregates at both 24 hours (P=0.0076) and 48 hours of
213 exposure (P=0.0364) (Fig. 2 c, d). The detection of aberrant a-syn accumulation in the SH-SY5Y
214 control line confirms that the observed increase was indeed driven by s-μg and not an exacerbation
215 of an existing defect, such as the 3K-SNCA mutation. Following the identification of increased

presence of a-syn aggregates, we questioned whether these findings were driven by a constitutive increase in the a-syn monomeric fraction, acting as a potential additional protein source and thereby promoting the formation of aggregated forms. To investigate the levels of a-syn monomers, we quantified the remaining a-syn signal that was not identified as an “aggregate” throughout the confocal microscopy screening. This assessment revealed a significant depletion of a-syn monomers in both 3K-SNCA cells (P=0.0145; P=0.0025) and SH-SY5Y cells (P=0.039; P=0.015) following s-μg exposure at both time points analyzed (Fig. 2 e, f).

To understand whether the observed increase in aggregated a-syn following s-μg exposure was accompanied an initial shift in pro-aggregation forms of the protein, we quantified the levels phosphorylated form on Serine-129 of a-syn (pS219). This phosphorylated form is a well-established marker of the aggregated state, as approximately 90% of a-synuclein in Lewy Bodies from PD brains contains pS129. Moreover, pS129 has been shown to accelerate the rate of a-syn fibrillation in vitro, suggesting that this specific phosphorylation event is closely linked to pathological aggregation.[69–71].

Initially, we conducted a comparative analysis between 1g SH-SY5Y cells and 1g 3K-SNCA cells to ascertain variations in pS219 presence. Our findings revealed a notably higher abundance of pS219 in 3K-SNCA cells compared to the wild-type model, substantiating and aligning with previous reports on the literature (data not shown) [72]. Levels of pS129 were significantly elevated in both cell types following exposure to s-μg, with this increase becoming more pronounced over the two time points analyzed (Fig. 3 a-d). These findings suggest that under s-μg conditions a-syn shifts from a non-aggregated status to phosphorylated and aggregated forms.

GCase is not increased in s-μg.

239 Given that s-μg may impact cellular processes, the abnormal behavior of a-syn observed under these
240 conditions might be due to disrupted lysosomal function, leading to impaired clearance and
241 increased aggregation of the protein. Thus, we hypothesized that this could be mechanistically
242 related to lysosomal dysfunction. To investigate this, we quantified the levels of GCase upon
243 exposition of the cells to s-μg conditions using the RPM. GCase was selected as it is an important
244 lysosomal enzyme in PD and a-syn turnover. Our analysis revealed that GCase levels were not
245 significantly altered at 24 or 48 hours (Fig. 4 a-d). We also measured Lysosomal-Associated
246 Membrane Protein 1 (LAMP1) levels as a reflection of lysosomal mass. Quantification of LAMP1
247 punctae using confocal microscopy revealed a significant increase in LAMP1-positive organelles over
248 time under s-μg conditions. Specifically, SH-SY5Y cells exhibited a more than 2-fold increase at both
249 24 hours (P=0.039) and 48 hours (P=0.025) of s-μg exposure. The PD model line 3K-SNCA presented
250 more variable levels of LAMP1, with a significant increase only present in exposure to s-μg at 48
251 hours (*P*=0.003). Although requiring further investigation, these results suggest that LAMP1 increase
252 may not be followed by a simultaneous increase in lysosomal hydrolases like GBA1, potentially
253 resulting in an impaired lysosomal maturation in s-μg.

254

255 ***ROS levels are increased in s-μg conditions***

256 When subjected to the s-μg induced by the random motion of the machine, both the 3K-SNCA
257 overexpressing cells and the control SH-SY5Y cells exhibited an elevated quantity of both monomeric
258 and aggregated states. An increase in oxidative stress is seen in the brain in several
259 neurodegenerative diseases including PD and has been noted in microgravity cell models
260 previously[56,57]. To investigate oxidative stress in our a-syn models, we quantified ROS and lipid
261 peroxidation levels in SH-SY5Y and 3K-SNCA cells exposed to s-μg conditions at 24 hours and 48
262 hours.

263 SH-SY5Y cells showed a significant 3-fold (*P*=0.019) and 2-fold increase (*P*=0.02) in ROS at 24 hours

264 and 48 hours respectively. Similarly, 3K-SNCA cells showed a significant increase of ROS cellular

265 content at both time points analysed (*P*=0.015; *P*=0.031) (Fig. 6 a, b).

266 We also measured MDA levels as an indicator of lipid peroxidation. MDA is generated by the
267 peroxidation of membrane polyunsaturated fatty acids [73] as well as produced in the process of
268 prostaglandin synthesis [74]. As s-μg conditions are a source of oxidative stress, s-μg also increases
269 MDA levels [75]. We exposed 3K-SNCA and SH-SY5Y cells to s-μg conditions for 24 and 48 hours,
270 using standard gravity exposed-cells as a control. There was no significant change in MDA levels in
271 the SH-SY5Y cells at either time point. In the 3K-SNCA, however, there was a significant 3-fold
272 increase (P=0.025) at 24 but not 48 hours (Fig. 6 c, d). These data are consistent with previous studies
273 showing that microgravity results in an increased presence of oxidative stress markers within the
274 cells. The failure of MDA levels to rise in the SH-SY5Y cells and the reversal of increased levels
275 between 24 and 48 hours in the 3K-SNCA cells suggests that compensatory mechanisms are
276 modulated in response to the increased ROS. For this, we investigate the levels of Catalase,
277 responsible of H_2O_2 hydrolysis, along with the TAC. However, we did not find any change in both
278 Catalase (Fig. S1 a-d) and TAC (Fig. S2 a-b) in either cell at any time point suggesting a potential
279 failure of antioxidant response despite the increased presence of ROS following s-μg exposure.

280

281 ***Discussion***

282 Microgravity research is increasingly recognized for its potential across various scientific disciplines.
283 While further investigation is needed to fully understand cellular adaptation to space-like conditions,
284 exploring how cells adjust to microgravity offers substantial promise for revealing diverse
285 pathophysiological processes [44,54,78,79]. In this study, s-μg was employed to simulate accelerated
286 aging, providing insights into the underlying pathophysiological mechanisms of PD. We report that
287 s-μg increases a-syn aggregate levels in both SH-SY5Y and 3K-SNCA cell models. Notably, exposure
288 to s-μg shifts the a-syn ratio towards aggregated form and increased pS129 modification, both
289 favoring the potential for Lewy body-like pathology [56,57].

290 All these observations could be attributed to s-μg induced cell stress, conceivably leading eventually
291 to a diminished clearance of a-syn, particularly pronounced in 3K-SNCA overexpressing cells. For this
292 reason, it was essential to investigate whether the increase in a-syn relates to compromised protein
293 clearance mechanisms, specifically involving autophagy–lysosome system dysfunction.

294 We hypothesised that lysosomal biogenesis was upregulated in s-μg as compensation for
295 accumulated a-syn aggregates. To evaluate this, we quantified both GCase lysosomal hydrolase as
296 well as LAMP1 in both cell types. Our analyses revealed that GCase levels remains unchanged, whilst
297 LAMP1 increases over time in both cell types. Several studies have demonstrated that GCase
298 homeostasis is affected by a-syn accumulation [32] by causing ER fragmentation and compromising
299 ER folding capacity and facilitating the aggregation of lysosomal hydrolases in the ER. The failure for
300 GCase levels to rise in our study may reflect this effect of a-syn, even against a compensatory attempt
301 to increase the endo-lysosomal content [30,31,46]. Accumulation of both a-syn and immature
302 lysosome hydrolases in the ER leads to activation of ER stress, thus evoking UPR [74,76] and resulting
303 in loss of ER homeostasis. This potentially culminates in ER dysfunction (changes in ER calcium
304 concentration or dysregulation in the redox potential of the ER) [77] or indirectly lysosomal catabolic
305 malfunction or mitochondrial abnormalities, which in turn could results in harmful oxidative damage
306 to the cells, and further a-syn aggregation [78,79].

307 In addition to this, ROS levels were increased in both cell types under s-μg conditions. Both s-μg and
308 a-syn aggregates accumulation are known to increase oxidative stress [19,80–82]. Additionally, a-
309 syn has been reported to suppress catalase activity [83]. These results suggests that cells exposed to
310 s-μg fail to activate protective mechanisms against rising levels of ROS, which may contribute to an
311 endo-lysosomal impairment, promoting GCase lysosomal hydrolase aberrant homeostasis,
312 potentially further facilitating a-synuclein aggregation.

313 Our findings describe a senescence model of PD cell pathology induced by microgravity, with
314 misfolded a-syn accumulation and oxidative stress. While the characteristics of the cell models used
315 in our study offer valuable insights for specific experimental contexts, they do not fully replicate the
316 complex cellular dynamics observed in PD. In contrast, differentiated cells, which more closely
317 resemble the specialized neuronal populations, would provide a more accurate representation of PD
318 pathological processes. These cells would better capture the scenario of neuronal dysfunction,
319 including the impact of a-syn aggregation and oxidative stress on cellular health and will be used in
320 future studies.

321

322 **Conclusions**

323 We report the first studies on the effect of s-μg on a-syn and show that it induces and enhances a-
324 syn accumulation in neuronal-type cells, accompanied by an increase in oxidative stress. These
325 findings provide valuable insights into cellular responses to s-μg, providing a basis for the usage of
326 s-μg and space-based experiments to model complex neurodegenerative disorders and ageing
327 features.

328

329 **Acknowledgments**

330 This work was funded by e.INS-Ecosystem of Innovation for Next Generation Sardinia (Grant ECS
331 00000038) funded by the Italian Ministry for Research and Education (MUR) under the National
332 Recovery and Resilience Plan (NRRP) MISSION 4COMPONENT 2, “From Research to Business” IN-
333 VEST-MENT 1.5, “Creation and Strengthening of Ecosystems of Innovation”, and construction of
334 “Territorial R&D Leaders”; by Aligning Science Across Parkinson’s [Grant number: ASAP000420]
335 through the Michael J. Fox Foundation for Parkinson’s Research; and the Sally Cohen Fund. For the

purpose of open access, the author has applied a CC BY 4.0 public copyright license to all Author Accepted Manuscripts arising from this submission.

Authors contributions

VL and GU contributed equally to this research. VL and GU conceived the study, designed and executed the analysis plan with supervision from GC, AP, and AHVS. GU, VL, AM, MAEF, and ND performed tissue culture work, immunostaining and data collection. VL and GU performed image analysis and conducted statistical analysis. AP and AHVS supported data interpretation. VL, GU, SLDP and AHVS wrote, designed, drafted and edited the manuscript with feedback and input from all authors. All authors read and approved the final manuscript.

Conflict of intertest

Nothing to report.

Data availability

The datasets in this study are not publicly available at the moment. They will be publicly available once the manuscript is accepted for publication.

Figures

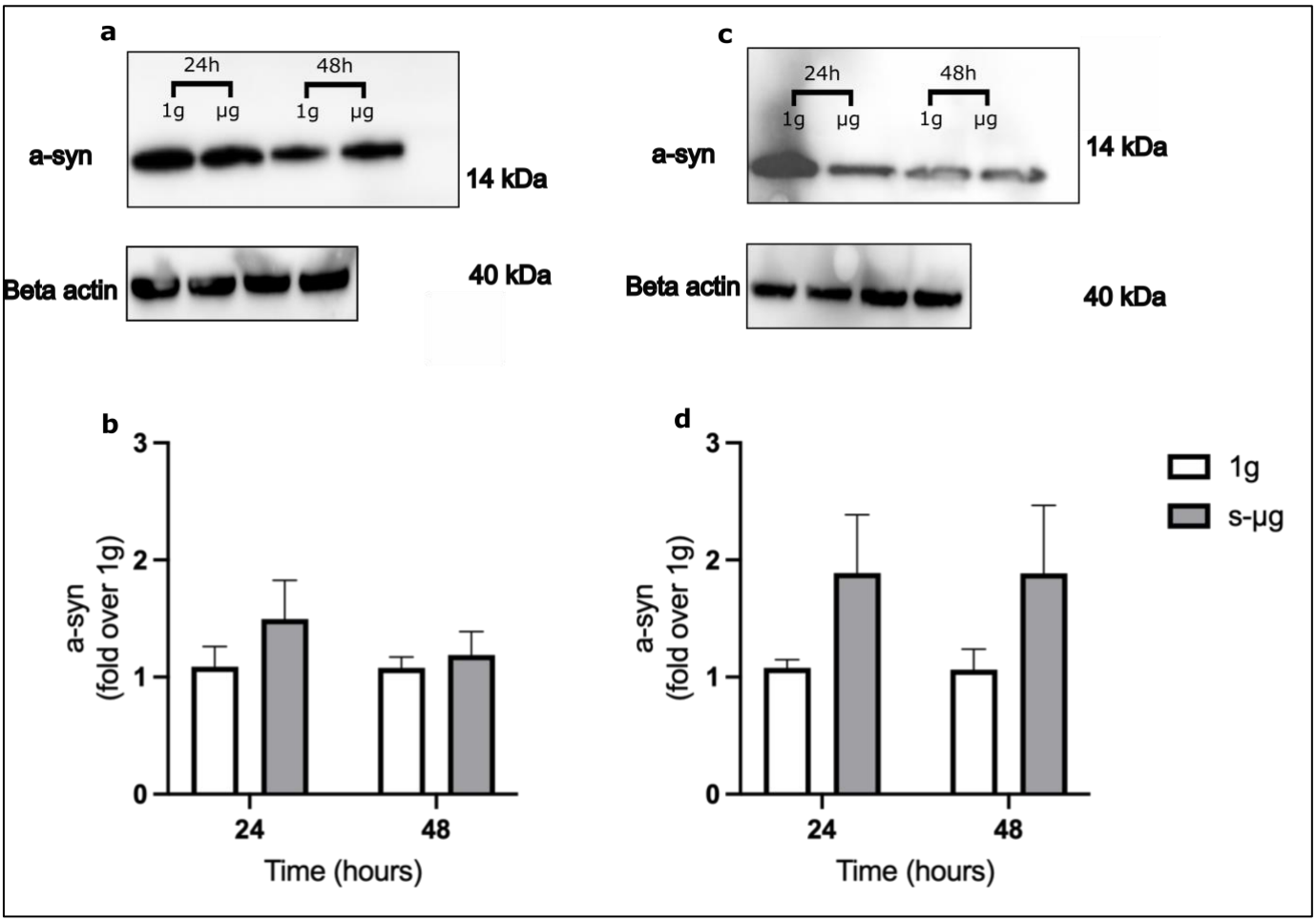

Figure 1. Total a-syn quantification in SH-SY5Y and 3K-SNCA cells exposed to s-mg conditions at different time points. a) Representative WB membrane image of a-syn and control protein beta-actin in SH-SY5Y cells. b) Quantification of a-syn levels in 1g and s-mg exposed SH-SY5Y cells. c) Representative WB membrane image of a-syn and control protein beta-actin in 3K-SNCA cells. d) Quantification of a-syn levels in 1g and s-mg exposed SH-SY5Y cells. Multiple unpaired t-tests were used to compare differences. Data are presented as mean±SEM of 3 independent experiments.

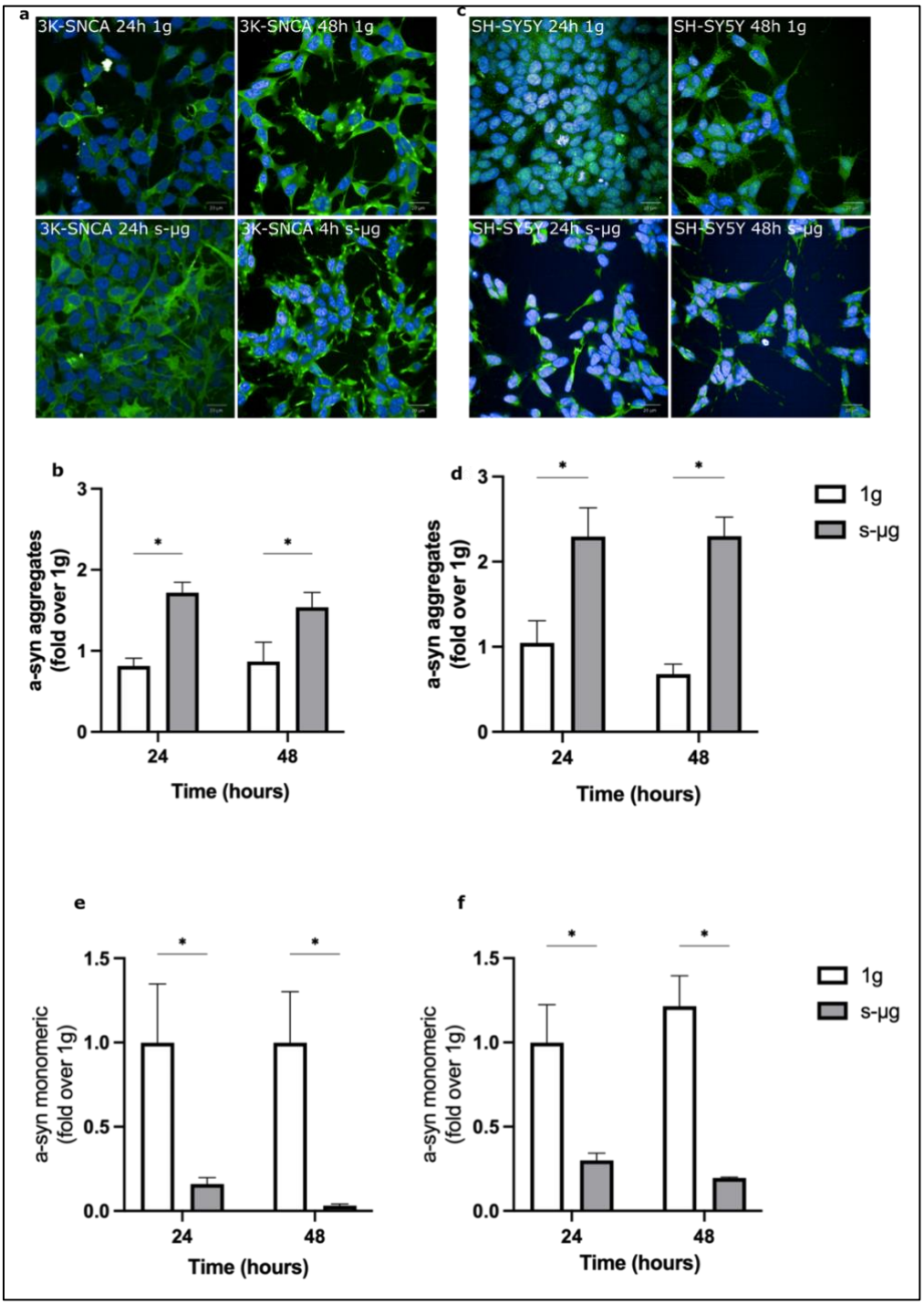

Figure 2. Quantification of a-syn aggregates via confocal microscopy in SH-SY5Y cells and 3K-SNCA cells. a-syn (green), Nuclei (blue). **a)** Representative confocal membrane images of a-syn aggregates in 3K-SNCA cells cultured in 1g and s-µg. **b)** Quantification of a-syn aggregates in 1g and s-µg exposed 3K-SNCA cells cultured in 1g and s-µg. **c)** Representative confocal images of a-syn aggregates in SH-SY5Y cells. **d)** Quantification of a-syn aggregates levels in 1g and s-µg exposed SH-SY5Y cells. **e)** Quantification of non-aggregated a-syn in 1g and s-µg exposed 3K-SNCA cells cultured in 1g and s-µg. **f)** Quantification of non-aggregated a-syn in 1g and s-µg exposed SH-SY5Y cells cultured in 1g and s-µg. Multiple unpaired t-tests were used to compare differences. Data are presented as mean±SEM of 3 independent experiments. *P<0.05

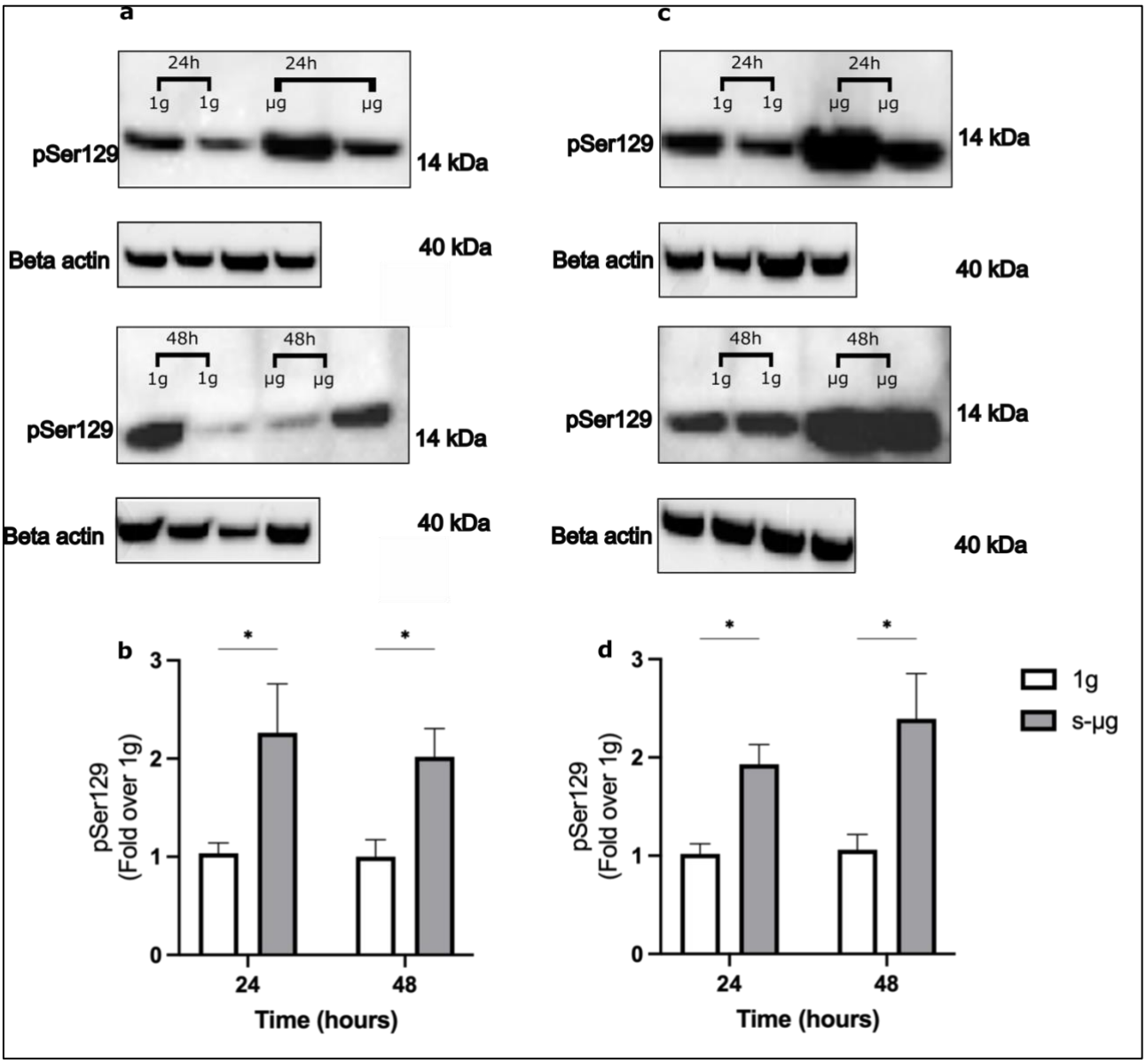

Figure 3. phosphorylated Serine 129 a-syn (pSer129) quantification in SH-SY5Y and 3K-SNCA cells exposed to s-µg at different time points. **a)** Representative WB membrane image of pSer129 and control protein beta-actin in SH-SY5Y cells. **b)** Quantification of pSer129 levels in 1g and s-µg exposed SH-SY5Y cells. **c)** Representative WB membrane image of pSer129 and control protein beta-actin in 3K-SNCA cells. **d)** Quantification of pSer129 levels in 1g and s-µg exposed SH-SY5Y cells. Multiple unpaired t-tests were used to compare differences. Data are presented as mean±SEM of 3 independent experiments. *$P<0.05$

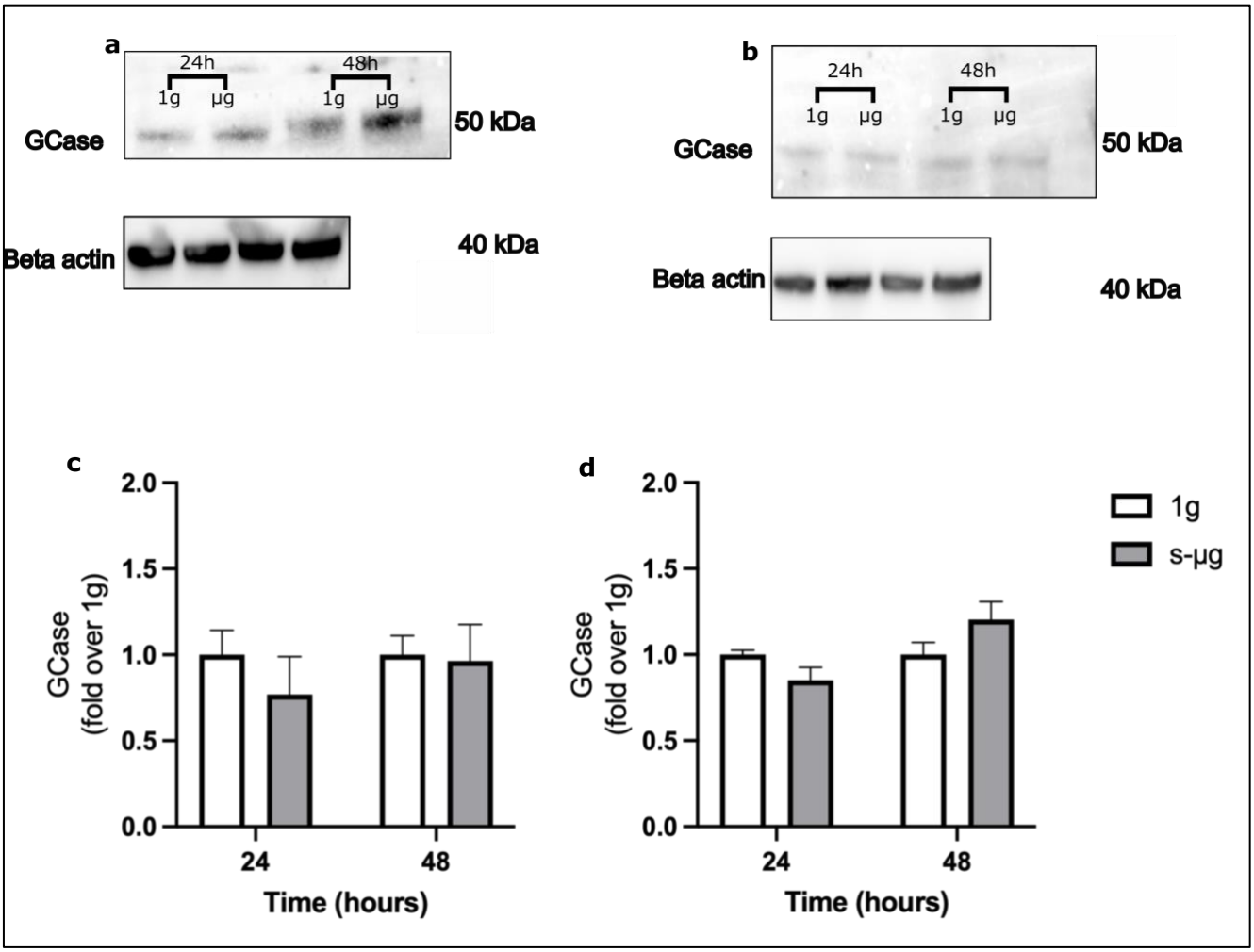

Figure 4. GCase WB quantification in SH-SY5Y and 3K-SNCA cells exposed to s-µg conditions at different time points. **a)** Representative WB membrane image of GCase and control protein beta-actin in SH-SY5Y cells. **b)** Quantification of GCase levels in 1g and s-µg exposed SH-SY5Y cells. **c)** Representative WB membrane image of GCase and control protein beta-actin in 3K-SNCA cells. **d)** Quantification of GCase levels in 1g and s-µg exposed SH-SY5Y cells. Multiple unpaired t-tests were used to compare differences. Data are presented as mean±SEM of 3 independent experiments.

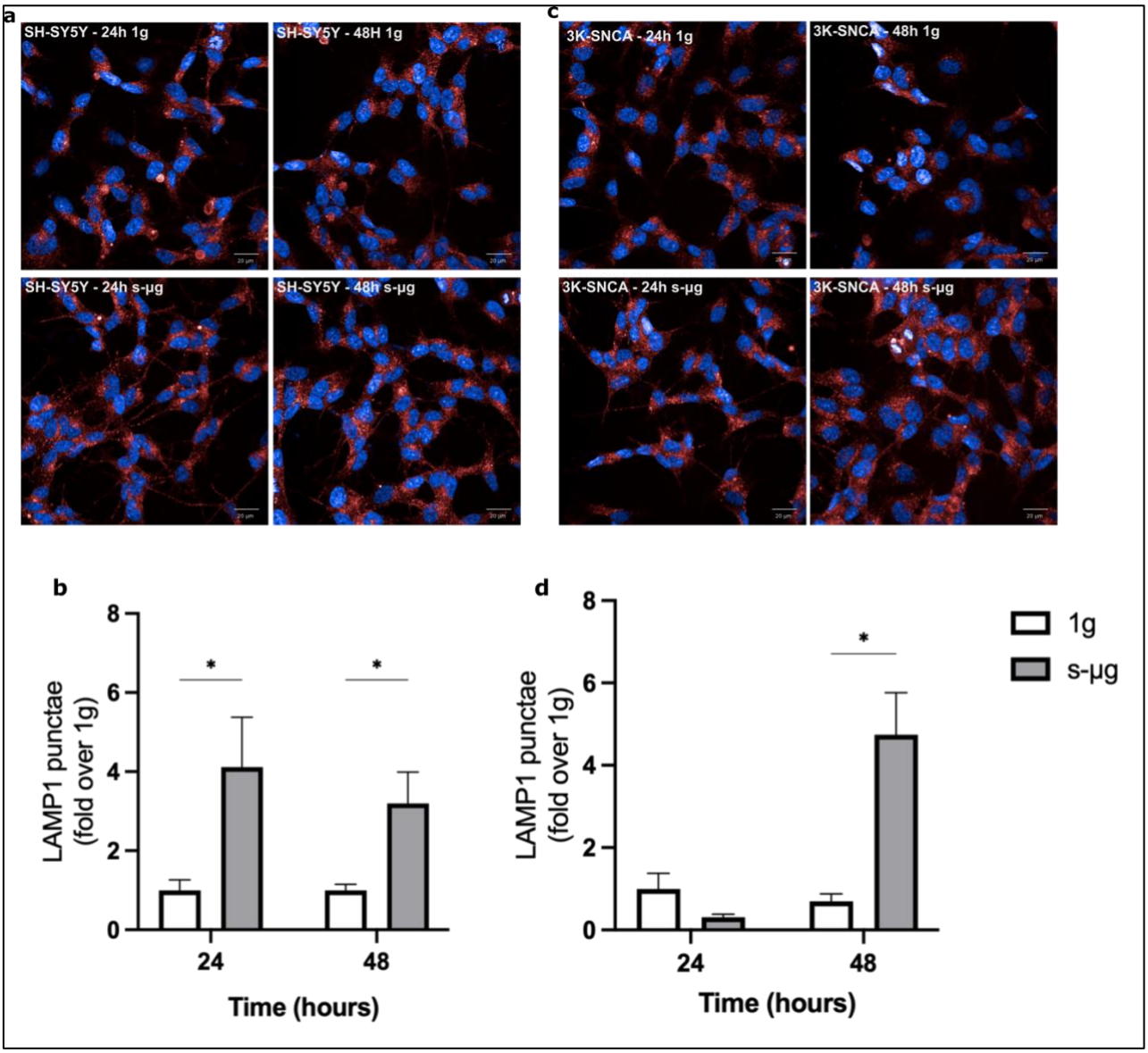

Figure 5. Quantification of LAMP1 punctae via confocal microscopy in SH-SY5Y cells and 3K-SNCA cells. LAMP1 (red), Nuclei (blue). **a)** Representative confocal membrane images of LAMP1 punctae in SH-SY5Y cells cultured in 1g and s-µg. **b)** Quantification of LAMP1 punctae in 1g and s-µg exposed SH-SY5Y cells. **c)** Representative confocal images of LAMP1 punctae in 3K-SNCA cells. **d)** Quantification of LAMP1 punctae levels in 1g and s-µg exposed 3K-SNCA cells. Multiple unpaired t-tests were used to compare differences. Data are presented as mean±SEM of 3 independent experiments. *$P<0.05$

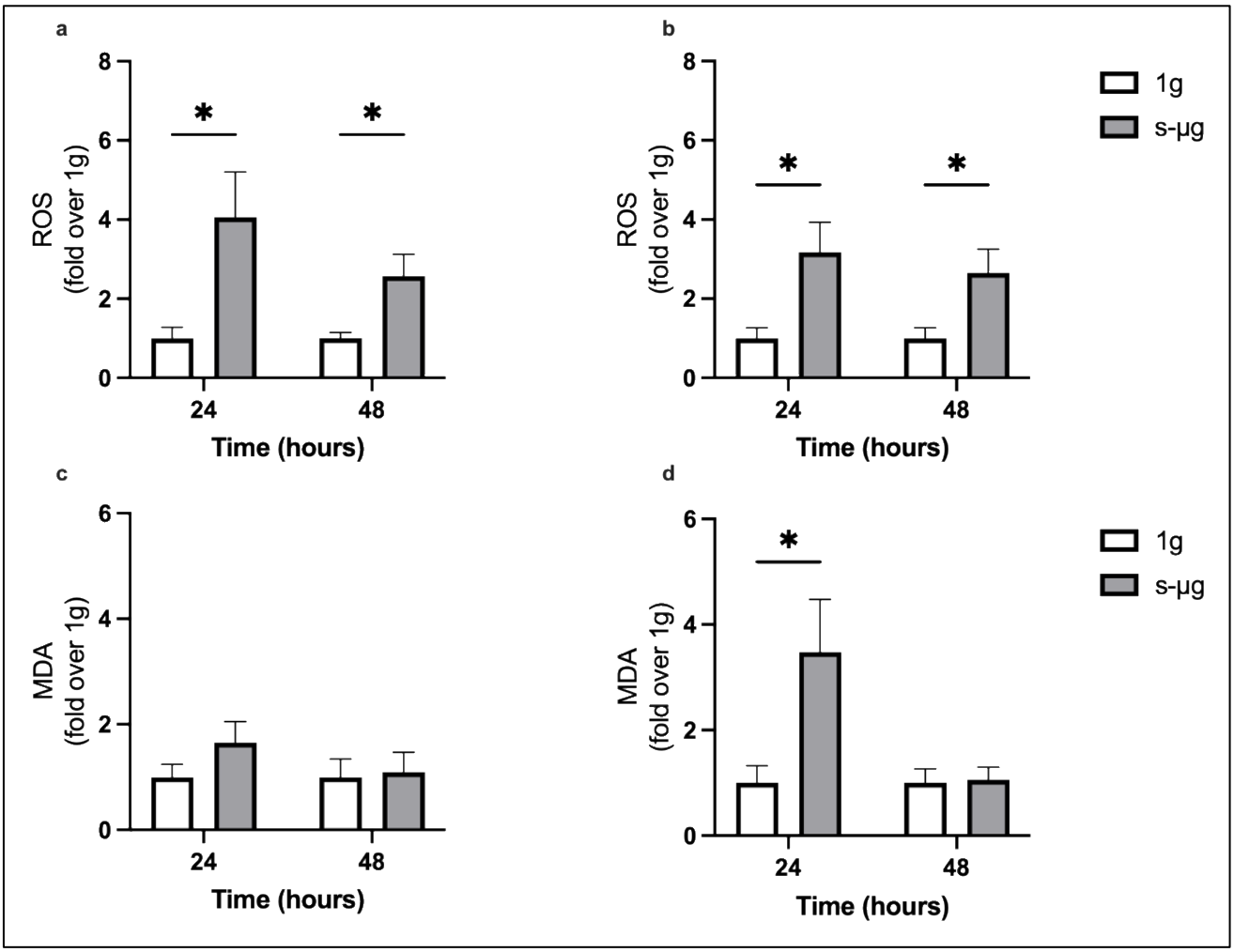

Figure 6. Investigation on oxidative stress marker in SH-SY5Y cells and 3K-SNCA cells exposed to s-µg. **a)** Quantification of ROS levels in SH-SY5Y cells cultured in 1g and s-µg. **b)** Quantification of ROS levels in 3K-SNCA cells cultured in 1g and s-µg. **c)** Quantification of MDA level in 1g and s-µg exposed SH-SY5Y cells. **d)** Quantification of MDA level in 1g and s-µg exposed 3K-SNCA cells. Multiple unpaired t-tests were used to compare differences. Data are presented as mean±SEM of 3 independent experiments. *P<0.05

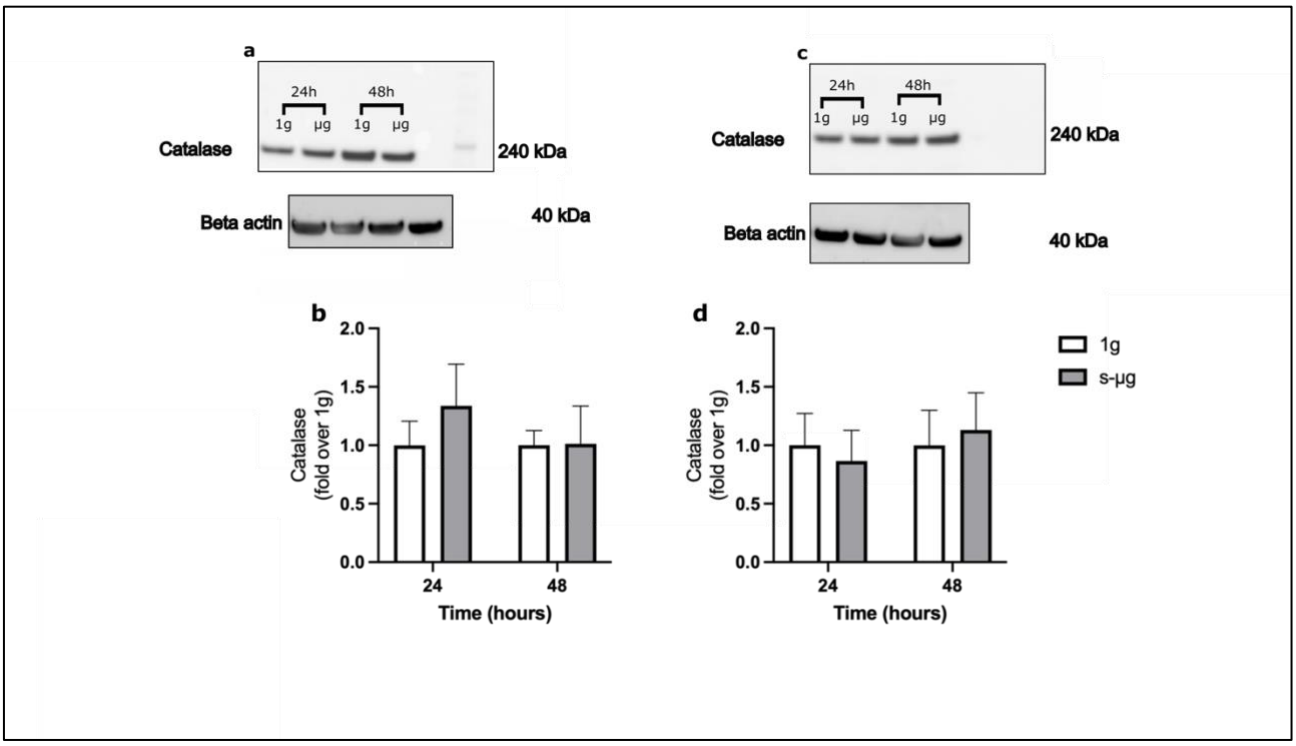

Figure S1. Catalase WB quantification in SH-SY5Y and 3K-SNCA cells exposed to s-µg at different time points. a) Representative WB membrane image of Catalase and control protein beta-actin in SH-SY5Y cells. b) Quantification of Catalase levels in 1g and s-µg exposed SH-SY5Y cells. c) Representative WB membrane image of Catalase and control protein beta-actin in 3K-SNCA cells. d) Quantification of Catalase levels in 1g and s-µg exposed SH-SY5Y cells. Multiple unpaired t-tests were used to compare differences. Data are presented as mean±SEM of 3 independent experiments.

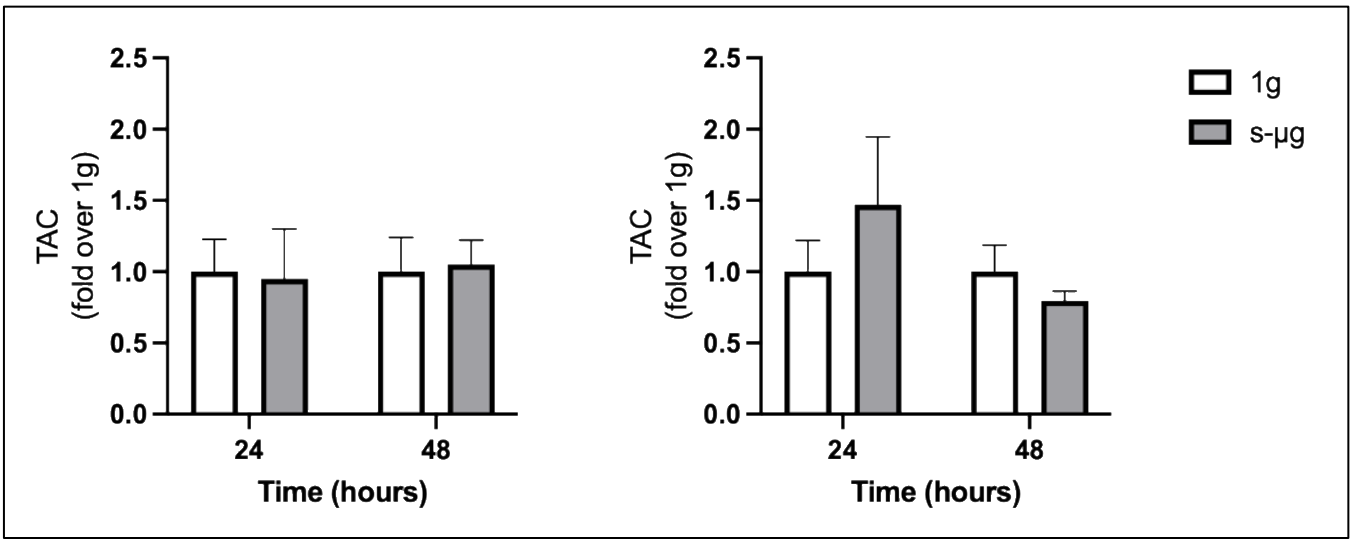

Figure S2. Investigation on total antioxidant capacity (TAC) in SH-SY5Y cells and 3K-SNCA cells exposed to s-µg. a) Quantification of TAC level in SH-SY5Y cells cultured in 1g and s-µg. b) Quantification of TAC level in 3K-SNCA cells cultured in 1g and s-µg. c) Quantification of TAC level in 1g and s-µg exposed SH-SY5Y cells. d) Quantification of TAC level in 1g and s-µg exposed 3K-SNCA cells. Multiple unpaired t-tests were used to compare differences. Data are presented as mean±SEM of 3 independent experiments.

Bibliography

1. Parkinson Disease Available online: https://www.who.int/news-room/fact-sheets/detail/parkinson-disease (accessed on 19 January 2023).

2. Postuma, R.B.; Berg, D.; Stern, M.; Poewe, W.; Olanow, C.W.; Oertel, W.; Obeso, J.; Marek, K.; Litvan, I.; Lang, A.E.; et al. MDS Clinical Diagnostic Criteria for Parkinson's Disease. *Movement Disorders* 2015, *30*.

3. Schapira, A.H.V.; Chaudhuri, K.R.; Jenner, P. Non-Motor Features of Parkinson Disease. *Nat Rev Neurosci* 2017, *18*.

4. Poewe, W.; Seppi, K.; Tanner, C.M.; Halliday, G.M.; Brundin, P.; Volkmann, J.; Schrag, A.E.; Lang, A.E. Parkinson Disease. *Nature Reviews Disease Primers 2017 3:1* **2017**, *3*, 1–21, doi:10.1038/nrdp.2017.13.

5. Balestrino, R.; Schapira, A.H.V. Parkinson Disease. *Eur J Neurol* **2020**, *27*, 27–42, doi:10.1111/ENE.14108.

6. Spillantini, M.G.; Schmidt, M.L.; Lee, V.M.Y.; Trojanowski, J.Q.; Jakes, R.; Goedert, M. α-Synuclein in Lewy Bodies [8]. *Nature* 1997, *388*.

7. Shahmoradian, S.H.; Lewis, A.J.; Genoud, C.; Hench, J.; Moors, T.E.; Navarro, P.P.; Castaño-Díez, D.; Schweighauser, G.; Graff-Meyer, A.; Goldie, K.N.; et al. Lewy Pathology in Parkinson's Disease Consists of Crowded Organelles and Lipid Membranes. *Nat Neurosci* **2019**, *22*, doi:10.1038/s41593-019-0423-2.

8. Mehra, S.; Sahay, S.; Maji, S.K. α-Synuclein Misfolding and Aggregation: Implications in Parkinson's Disease Pathogenesis. *Biochim Biophys Acta Proteins Proteom* 2019, *1867*.

9. Polymeropoulos, M.H.; Lavedan, C.; Leroy, E.; Ide, S.E.; Dehejia, A.; Dutra, A.; Pike, B.; Root, H.; Rubenstein, J.; Boyer, R.; et al. Mutation in the Alpha-Synuclein Gene Identified in Families with Parkinson's Disease. *Science* **1997**, *276*, 2045–2047, doi:10.1126/SCIENCE.276.5321.2045.

10. Singleton, A.B.; Farrer, M.; Johnson, J.; Singleton, A.; Hague, S.; Kachergus, J.; Hulihan, M.; Peuralinna, T.; Dutra, A.; Nussbaum, R.; et al. Alpha-Synuclein Locus Triplication Causes Parkinson's Disease. *Science* **2003**, *302*, 841, doi:10.1126/SCIENCE.1090278.

11. Sidransky, E.; Nalls, M.A.; Aasly, J.O.; Aharon-Peretz, J.; Annesi, G.; Barbosa, E.R.; Bar-Shira, A.; Berg, D.; Bras, J.; Brice, A.; et al. Multicenter Analysis of Glucocerebrosidase Mutations in Parkinson's Disease. *N Engl J Med* **2009**, *361*, 1651–1661, doi:10.1056/NEJMOA0901281.

12. Tan, E.K.; Yew, K.; Chua, E.; Puvan, K.; Shen, H.; Lee, E.; Puong, K.Y.; Zhao, Y.; Pavanni, R.; Wong, M.C.; et al. PINK1 Mutations in Sporadic Early-Onset Parkinson's Disease. *Movement Disorders* **2006**, *21*, 789–793, doi:10.1002/MDS.20810.

13. Kitada, T.; Asakawa, S.; Hattori, N.; Matsumine, H.; Yamamura, Y.; Minoshima, S.; Yokochi, M.; Mizuno, Y.; Shimizu, N. Mutations in the Parkin Gene Cause Autosomal Recessive Juvenile Parkinsonism. *Nature 1998 392:6676* **1998**, *392*, 605–608, doi:10.1038/33416.

14. Zimprich, A.; Biskup, S.; Leitner, P.; Lichtner, P.; Farrer, M.; Lincoln, S.; Kachergus, J.; Hulihan, M.; Uitti, R.J.; Calne, D.B.; et al. Mutations in LRRK2 Cause Autosomal-Dominant Parkinsonism with Pleomorphic Pathology. *Neuron* **2004**, *44*, 601–607, doi:10.1016/J.NEURON.2004.11.005.

529 15. Schapira, A.H.; Jenner, P. Etiology and Pathogenesis of Parkinson's Disease. *Movement Disorders*
530 **2011**, *26*, 1049–1055, doi:10.1002/MDS.23732.

531 16. Berent, S.L.; Radin, N.S. Mechanism of Activation of Glucocerebrosidase by CO-β-Glucosidase
532 (Glucosidase Activator Protein). *Biochimica et Biophysica Acta (BBA)/Lipids and Lipid Metabolism*
533 **1981**, *664*, doi:10.1016/0005-2760(81)90134-X.

534 17. Bendor, J.T.; Logan, T.P.; Edwards, R.H. The Function of α-Synuclein. *Neuron* 2013, *79*.

535 18. Du, X.Y.; Xie, X.X.; Liu, R.T. The Role of α-Synuclein Oligomers in Parkinson's Disease. *Int J Mol Sci*
536 **2020**, *21*, 1–17, doi:10.3390/IJMS21228645.

537 19. Deas, E.; Cremades, N.; Angelova, P.R.; Ludtmann, M.H.R.; Yao, Z.; Chen, S.; Horrocks, M.H.; Banushi,
538 B.; Little, D.; Devine, M.J.; et al. Alpha-Synuclein Oligomers Interact with Metal Ions to Induce
539 Oxidative Stress and Neuronal Death in Parkinson's Disease. *Antioxid Redox Signal* **2016**, *24*, 376–
540 391, doi:10.1089/ARS.2015.6343.

541 20. Tanik, S.A.; Schultheiss, C.E.; Volpicelli-Daley, L.A.; Brunden, K.R.; Lee, V.M.Y. Lewy Body-like α-
542 Synuclein Aggregates Resist Degradation and Impair Macroautophagy. *Journal of Biological*
543 *Chemistry* **2013**, *288*, doi:10.1074/jbc.M113.457408.

544 21. Ebrahimi-Fakhari, D.; Cantuti-Castelvetri, I.; Fan, Z.; Rockenstein, E.; Masliah, E.; Hyman, B.T.;
545 McLean, P.J.; Unni, V.K. Distinct Roles in Vivo for the Ubiquitin-Proteasome System and the
546 Autophagy-Lysosomal Pathway in the Degradation of α-Synuclein. *Journal of Neuroscience* **2011**, *31*,
547 doi:10.1523/JNEUROSCI.1560-11.2011.

548 22. Vogiatzi, T.; Xilouri, M.; Vekrellis, K.; Stefanis, L. Wild Type α-Synuclein Is Degraded by Chaperone-
549 Mediated Autophagy and Macroautophagy in Neuronal Cells. *Journal of Biological Chemistry* **2008**,
550 *283*, doi:10.1074/jbc.M801992200.

551 23. Cuervo, A.M.; Stafanis, L.; Fredenburg, R.; Lansbury, P.T.; Sulzer, D. Impaired Degradation of Mutant
552 α-Synuclein by Chaperone-Mediated Autophagy. *Science (1979)* **2004**, *305*,
553 doi:10.1126/science.1101738.

554 24. Wallings, R.L.; Humble, S.W.; Ward, M.E.; Wade-Martins, R. Lysosomal Dysfunction at the Centre of
555 Parkinson's Disease and Frontotemporal Dementia/Amyotrophic Lateral Sclerosis. *Trends Neurosci*
556 2019, *42*.

557 25. Alvarez-Erviti, L.; Rodriguez-Oroz, M.C.; Cooper, J.M.; Caballero, C.; Ferrer, I.; Obeso, J.A.; Schapira,
558 A.H.V. Chaperone-Mediated Autophagy Markers in Parkinson Disease Brains. *Arch Neurol* **2010**, *67*,
559 doi:10.1001/archneurol.2010.198.

560 26. Gegg, M.E.; Burke, D.; Heales, S.J.R.; Cooper, J.M.; Hardy, J.; Wood, N.W.; Schapira, A.H.V.
561 Glucocerebrosidase Deficiency in Substantia Nigra of Parkinson Disease Brains. *Ann Neurol* **2012**, *72*,
562 455–463, doi:10.1002/ANA.23614.

563 27. Sidransky, E.; Lopez, G. The Link between the GBA Gene and Parkinsonism. *Lancet Neurol* **2012**, *11*,
564 doi:10.1016/S1474-4422(12)70190-4.

565 28. Kuo, S.H.; Tasset, I.; Cheng, M.M.; Diaz, A.; Pan, M.K.; Lieberman, O.J.; Hutten, S.J.; Alcalay, R.N.; Kim,
566 S.; Ximénez-Embún, P.; et al. Mutant Glucocerebrosidase Impairs α-Synuclein Degradation by
567 Blockade of Chaperone-Mediated Autophagy. *Sci Adv* **2022**, *8*, doi:10.1126/sciadv.abm6393.

568 29. Mazzulli, J.R.; Zunke, F.; Tsunemi, T.; Toker, N.J.; Jeon, S.; Burbulla, L.F.; Patnaik, S.; Sidransky, E.;
569 Marugan, J.J.; Sue, C.M.; et al. Activation of β-Glucocerebrosidase Reduces Pathological α-Synuclein

and Restores Lysosomal Function in Parkinson's Patient Midbrain Neurons. *Journal of Neuroscience* **2016**, *36*, doi:10.1523/JNEUROSCI.0628-16.2016.

30. García-Sanz, P.; Orgaz, L.; Fuentes, J.M.; Vicario, C.; Moratalla, R. Cholesterol and Multilamellar Bodies: Lysosomal Dysfunction in GBA-Parkinson Disease. *Autophagy* 2018, *14*.

31. García-Sanz, P.; Orgaz, L.; Bueno-Gil, G.; Espadas, I.; Rodríguez-Traver, E.; Kulisevsky, J.; Gutierrez, A.; Dávila, J.C.; González-Polo, R.A.; Fuentes, J.M.; et al. N370S-GBA1 Mutation Causes Lysosomal Cholesterol Accumulation in Parkinson's Disease. *Movement Disorders* **2017**, *32*, doi:10.1002/mds.27119.

32. Stojkovska, I.; Wani, W.Y.; Zunke, F.; Belur, N.R.; Pavlenko, E.A.; Mwenda, N.; Sharma, K.; Francelle, L.; Mazzulli, J.R. Rescue of α-Synuclein Aggregation in Parkinson's Patient Neurons by Synergistic Enhancement of ER Proteostasis and Protein Trafficking. *Neuron* **2022**, *110*, doi:10.1016/j.neuron.2021.10.032.

33. Smith, L.; Schapira, A.H.V. GBA Variants and Parkinson Disease: Mechanisms and Treatments. *Cells 2022, Vol. 11, Page 1261* **2022**, *11*, 1261, doi:10.3390/CELLS11081261.

34. Behl, T.; Kaur, G.; Fratila, O.; Buhas, C.; Judea-Pusta, C.T.; Negrut, N.; Bustea, C.; Bungau, S. Cross-Talks among GBA Mutations, Glucocerebrosidase, and α-Synuclein in GBA-Associated Parkinson's Disease and Their Targeted Therapeutic Approaches: A Comprehensive Review. *Translational Neurodegeneration 2021 10:1* **2021**, *10*, 1–13, doi:10.1186/S40035-020-00226-X.

35. Henderson, M.X.; Cornblath, E.J.; Darwich, A.; Zhang, B.; Brown, H.; Gathagan, R.J.; Sandler, R.M.; Bassett, D.S.; Trojanowski, J.Q.; Lee, V.M.Y. Spread of α-Synuclein Pathology through the Brain Connectome Is Modulated by Selective Vulnerability and Predicted by Network Analysis. *Nat Neurosci* **2019**, *22*, doi:10.1038/s41593-019-0457-5.

36. Mazzulli, J.R.; Xu, Y.H.; Sun, Y.; Knight, A.L.; McLean, P.J.; Caldwell, G.A.; Sidransky, E.; Grabowski, G.A.; Krainc, D. Gaucher Disease Glucocerebrosidase and α-Synuclein Form a Bidirectional Pathogenic Loop in Synucleinopathies. *Cell* **2011**, *146*, doi:10.1016/j.cell.2011.06.001.

37. Colla, E. Linking the Endoplasmic Reticulum to Parkinson's Disease and Alpha-Synucleinopathy. *Front Neurosci* **2019**, *13*, doi:10.3389/fnins.2019.00560.

38. Smith, W.W.; Jiang, H.; Pei, Z.; Tanaka, Y.; Morita, H.; Sawa, A.; Dawson, V.L.; Dawson, T.M.; Ross, C.A. Endoplasmic Reticulum Stress and Mitochondrial Cell Death Pathways Mediate A53T Mutant Alpha-Synuclein-Induced Toxicity. *Hum Mol Genet* **2005**, *14*, doi:10.1093/hmg/ddi396.

39. Heman-Ackah, S.M.; Manzano, R.; Hoozemans, J.J.M.; Scheper, W.; Flynn, R.; Haerty, W.; Cowley, S.A.; Bassett, A.R.; Wood, M.J.A. Alpha-Synuclein Induces the Unfolded Protein Response in Parkinson's Disease SNCA Triplication IPSC-Derived Neurons. *Hum Mol Genet* **2017**, *26*, doi:10.1093/hmg/ddx331.

40. Smith, J.K. Osteoclasts and Microgravity. *Life 2020, Vol. 10, Page 207* **2020**, *10*, 207, doi:10.3390/LIFE10090207.

41. Buoite Stella, A.; Ajčević, M.; Furlanis, G.; Manganotti, P. Neurophysiological Adaptations to Spaceflight and Simulated Microgravity. *Clin Neurophysiol* **2021**, *132*, 498–504, doi:10.1016/J.CLINPH.2020.11.033.

42. Juhl, O.J.; Buettmann, E.G.; Friedman, M.A.; DeNapoli, R.C.; Hoppock, G.A.; Donahue, H.J. Update on the Effects of Microgravity on the Musculoskeletal System. *npj Microgravity 2021 7:1* **2021**, *7*, 1–15, doi:10.1038/s41526-021-00158-4.

43. Wu, X.T.; Yang, X.; Tian, R.; Li, Y.H.; Wang, C.Y.; Fan, Y.B.; Sun, L.W. Cells Respond to Space Microgravity through Cytoskeleton Reorganization. *FASEB Journal* **2022**, *36*, doi:10.1096/FJ.202101140R.

44. Nguyen, H.P.; Tran, P.H.; Kim, K.S.; Yang, S.G. The Effects of Real and Simulated Microgravity on Cellular Mitochondrial Function. *npj Microgravity 2021 7:1* **2021**, *7*, 1–11, doi:10.1038/s41526-021-00171-7.

45. Amselem, S. Remote Controlled Autonomous Microgravity Lab Platforms for Drug Research in Space. *Pharm Res* **2019**, *36*, 1–15, doi:10.1007/S11095-019-2703-7/FIGURES/8.

46. Roy-O'Reilly, M.; Mulavara, A.; Williams, T. A Review of Alterations to the Brain during Spaceflight and the Potential Relevance to Crew in Long-Duration Space Exploration. *NPJ Microgravity* **2021**, *7*, doi:10.1038/S41526-021-00133-Z.

47. Stavnichuk, M.; Mikolajewicz, N.; Corlett, T.; Morris, M.; Komarova, S. V. A Systematic Review and Meta-Analysis of Bone Loss in Space Travelers. *NPJ Microgravity* **2020**, *6*, doi:10.1038/S41526-020-0103-2.

48. Frippiat, J.P.; Crucian, B.E.; de Quervain, D.J.F.; Grimm, D.; Montano, N.; Praun, S.; Roozendaal, B.; Schelling, G.; Thiel, M.; Ullrich, O.; et al. Towards Human Exploration of Space: The THESEUS Review Series on Immunology Research Priorities. *NPJ Microgravity* **2016**, *2*, doi:10.1038/NPJMGRAV.2016.40.

49. Tauber, S.; Hauschild, S.; Paulsen, K.; Gutewort, A.; Raig, C.; Hürlimann, E.; Biskup, J.; Philpot, C.; Lier, H.; Engelmann, F.; et al. Signal Transduction in Primary Human T Lymphocytes in Altered Gravity During Parabolic Flight and Clinostat Experiments. *Cellular Physiology and Biochemistry* **2015**, *35*, 1034–1051, doi:10.1159/000373930.

50. Zhang, Y.; Wang, H.; Lai, C.; Wang, L.; Deng, Y. Comparative Proteomic Analysis of Human SH-SY5Y Neuroblastoma Cells under Simulated Microgravity. *Astrobiology* **2013**, *13*, 143–150, doi:10.1089/AST.2012.0822/ASSET/IMAGES/LARGE/FIGURE7.JPEG.

51. Rampoldi, A.; Forghani, P.; Li, D.; Hwang, H.; Armand, L.C.; Fite, J.; Boland, G.; Maxwell, J.; Maher, K.; Xu, C. Space Microgravity Improves Proliferation of Human IPSC-Derived Cardiomyocytes. *Stem Cell Reports* **2022**, *17*, doi:10.1016/j.stemcr.2022.08.007.

52. Striebel, J.; Kalinski, L.; Sturm, M.; Drouvé, N.; Peters, S.; Lichterfeld, Y.; Habibey, R.; Hauslage, J.; El Sheikh, S.; Busskamp, V.; et al. Human Neural Network Activity Reacts to Gravity Changes in Vitro. *Front Neurosci* **2023**, *17*, doi:10.3389/fnins.2023.1085282.

53. Wang, J.; Zhang, J.; Bai, S.; Wang, G.; Mu, L.; Sun, B.; Wang, D.; Kong, Q.; Liu, Y.; Yao, X.; et al. Simulated Microgravity Promotes Cellular Senescence via Oxidant Stress in Rat PC12 Cells. *Neurochem Int* **2009**, *55*, 710–716, doi:10.1016/J.NEUINT.2009.07.002.

54. Pala, R.; Cruciani, S.; Manca, A.; Garroni, G.; EL Faqir, M.A.; Lentini, V.; Capobianco, G.; Pantaleo, A.; Maioli, M. Mesenchymal Stem Cell Behavior under Microgravity: From Stress Response to a Premature Senescence. *Int J Mol Sci* **2023**, *24*, doi:10.3390/IJMS24097753.

55. Di Giulio, C. Do We Age Faster in Absence of Gravity? *Front Physiol* **2013**, *4*, doi:10.3389/FPHYS.2013.00134.

56. Fukuda, A.; … V. de L.C.-L.S. in S.; 2021, undefined Simulated Microgravity Accelerates Aging in Saccharomyces Cerevisiae. *Elsevier*.

57. Dinarelli, S.; Longo, G.; Dietler, G.; Francioso, A.; Mosca, L.; Pannitteri, G.; Boumis, G.; Bellelli, A.; Girasole, & M. Erythrocyte's Aging in Microgravity Highlights How Environmental Stimuli Shape Metabolism and Morphology. *Springer* **2018**, *8*, 5277, doi:10.1038/s41598-018-22870-0.

58. Ratushnyy, A.Y.; Buravkova, L.B. Microgravity Effects and Aging Physiology: Similar Changes or Common Mechanisms? *Biochemistry (Moscow)* 2023, *88*, 1763–1777.

59. Prasad, B.; Grimm, D.; Strauch, S.M.; Erzinger, G.S.; Corydon, T.J.; Lebert, M.; Magnusson, N.E.; Infanger, M.; Richter, P.; Krüger, M. Influence of Microgravity on Apoptosis in Cells, Tissues, and Other Systems in Vivo and in Vitro. *Int J Mol Sci* **2020**, *21*, doi:10.3390/ijms21249373.

60. Uras, G.; Li, X.; Manca, A.; Pantaleo, A.; Bo, M.; Xu, J.; Allen, S.; Zhu, Z. Development of P-Tau Differentiated Cell Model of Alzheimer's Disease to Screen Novel Acetylcholinesterase Inhibitors. *Int J Mol Sci* **2022**, *23*, 14794, doi:10.3390/IJMS232314794/S1.

61. Xicoy, H.; Wieringa, B.; Martens, G.J.M. The SH-SY5Y Cell Line in Parkinson's Disease Research: A Systematic Review. *Mol Neurodegener* 2017, *12*.

62. Lucas-Del-Pozo, #; Sara; Uras, ; #; Giuseppe; Fierli, ; Federico; Lentini, ; Veronica; Koletsi, ; Sofia; et al. Reduction of A-Synuclein Aggregates by PIKfyve Inhibition via TFEB-Mediated Lysosomal Biogenesis in a Parkinson Disease Model. *bioRxiv* **2023**, 2023.10.23.563557, doi:10.1101/2023.10.23.563557.

63. Terry-Kantor, E.; Tripathi, A.; Imberdis, T.; Lavoie, Z.M.; Ho, G.P.H.; Selkoe, D.; Fanning, S.; Ramalingam, N.; Dettmer, U. Rapid Alpha-Synuclein Toxicity in a Neural Cell Model and Its Rescue by a Stearoyl-CoA Desaturase Inhibitor. *International Journal of Molecular Sciences 2020, Vol. 21, Page 5193* **2020**, *21*, 5193, doi:10.3390/IJMS21155193.

64. Wuest, S.L.; Richard, S.; Kopp, S.; Grimm, D.; Egli, M. Simulated Microgravity: Critical Review on the Use of Random Positioning Machines for Mammalian Cell Culture. *Biomed Res Int* 2015, *2015*.

65. Bradshaw, A. V.; Campbell, P.; Schapira, A.H.V.; Morris, H.R.; Taanman, J.W. The PINK1-Parkin Mitophagy Signalling Pathway Is Not Functional in Peripheral Blood Mononuclear Cells. *PLoS One* **2021**, *16*, doi:10.1371/journal.pone.0259903.

66. Uras, G. *Evaluation of AChE Inhibitors and Dual AChE/GSK3-β Inhibitor as Alzheimer's Disease Treatment*;

67. Costa, C.A. da; Manaa, W. El; Duplan, E.; Checler, F. The Endoplasmic Reticulum Stress/Unfolded Protein Response and Their Contributions to Parkinson's Disease Physiopathology. *Cells 2020, Vol. 9, Page 2495* **2020**, *9*, 2495, doi:10.3390/CELLS9112495.

68. Colla, E. Linking the Endoplasmic Reticulum to Parkinson's Disease and Alpha-Synucleinopathy. *Front Neurosci* **2019**, *13*, 461767, doi:10.3389/FNINS.2019.00560/BIBTEX.

69. Kawahata, I.; Finkelstein, D.I.; Fukunaga, K. Pathogenic Impact of α-Synuclein Phosphorylation and Its Kinases in α-Synucleinopathies. *International Journal of Molecular Sciences 2022, Vol. 23, Page 6216* **2022**, *23*, 6216, doi:10.3390/IJMS23116216.

70. Stewart, T.; Sossi, V.; Aasly, J.O.; Wszolek, Z.K.; Uitti, R.J.; Hasegawa, K.; Yokoyama, T.; Zabetian, C.P.; Leverenz, J.B.; Stoessl, A.J.; et al. Phosphorylated α-Synuclein in Parkinson's Disease: Correlation Depends on Disease Severity. *Acta Neuropathol Commun* **2015**, *3*, 7, doi:10.1186/S40478-015-0185-3/FIGURES/3.

71. Fujiwara, H.; Hasegawa, M.; Dohmae, N.; Kawashima, A.; Masliah, E.; Goldberg, M.S.; Shen, J.; Takio, K.; Iwatsubo, T. α-Synuclein Is Phosphorylated in Synucleinopathy Lesions. *Nat Cell Biol* **2002**, *4*, doi:10.1038/ncb748.

72. Mbefo, M.K.; Fares, M.B.; Paleologou, K.; Oueslati, A.; Yin, G.; Tenreiro, S.; Pinto, M.; Outeiro, T.; Zweckstetter, M.; Masliah, E.; et al. Parkinson Disease Mutant E46K Enhances α-Synuclein Phosphorylation in Mammalian Cell Lines, in Yeast, and in Vivo. *J Biol Chem* **2015**, *290*, 9412, doi:10.1074/JBC.M114.610774.

73. Esterbauer, H.; Schaur, R.J.; Zollner, H. Chemistry and Biochemistry of 4-Hydroxynonenal, Malonaldehyde and Related Aldehydes. *Free Radic Biol Med* 1991, *11*.

74. Marnett, L.J. Oxy Radicals, Lipid Peroxidation and DNA Damage. *Toxicology* **2002**, *181–182*, doi:10.1016/S0300-483X(02)00448-1.

75. Zhang, Y.; Wang, H.; Lai, C.; Wang, L.; Deng, Y. Comparative Proteomic Analysis of Human SH-SY5Y Neuroblastoma Cells under Simulated Microgravity. *https://home.liebertpub.com/ast* **2013**, *13*, 143–150, doi:10.1089/AST.2012.0822.

76. Colla, E.; Coune, P.; Liu, Y.; Pletnikova, O.; Troncoso, J.C.; Iwatsubo, T.; Schneider, B.L.; Lee, M.K. Endoplasmic Reticulum Stress Is Important for the Manifestations of α-Synucleinopathy in Vivo. *Journal of Neuroscience* **2012**, *32*, doi:10.1523/JNEUROSCI.5367-11.2012.

77. Kim, S.; Kim, D.K.; Jeong, S.; Lee, J. The Common Cellular Events in the Neurodegenerative Diseases and the Associated Role of Endoplasmic Reticulum Stress. *Int J Mol Sci* 2022, *23*.

78. Karvandi, M.S.; Sheikhzadeh Hesari, F.; Aref, A.R.; Mahdavi, M. The Neuroprotective Effects of Targeting Key Factors of Neuronal Cell Death in Neurodegenerative Diseases: The Role of ER Stress, Oxidative Stress, and Neuroinflammation. *Front Cell Neurosci* 2023, *17*.

79. Chou, S.M.; Yen, Y.H.; Yuan, F.; Zhang, S.C.; Chong, C.M. Neuronal Senescence in the Aged Brain. *Aging Dis* 2023, *14*.

80. Byers, B.; Cord, B.; Nguyen, H.N.; Schüle, B.; Fenno, L.; Lee, P.C.; Deisseroth, K.; Langston, J.W.; Pera, R.R.; Palmer, T.D. SNCA Triplication Parkinson's Patient's IPSC-Derived DA Neurons Accumulate α-Synuclein and Are Susceptible to Oxidative Stress. *PLoS One* **2011**, *6*, e26159, doi:10.1371/JOURNAL.PONE.0026159.

81. Nguyen, H.N.; Byers, B.; Cord, B.; Shcheglovitov, A.; Byrne, J.; Gujar, P.; Kee, K.; Schüle, B.; Dolmetsch, R.E.; Langston, W.; et al. LRRK2 Mutant IPSC-Derived DA Neurons Demonstrate Increased Susceptibility to Oxidative Stress. *Cell Stem Cell* **2011**, *8*, 267–280, doi:10.1016/J.STEM.2011.01.013.

82. Manis, C.; Manca, A.; Murgia, A.; Uras, G.; Caboni, P.; Congiu, T.; Faa, G.; Pantaleo, A.; Cao, G. Understanding the Behaviour of Human Cell Types under Simulated Microgravity Conditions: The Case of Erythrocytes. *Int J Mol Sci* **2022**, *23*, doi:10.3390/ijms23126876.

83. Yakunin, E.; Kisos, H.; Kulik, W.; Grigoletto, J.; Wanders, R.J.A.; Sharon, R. The Regulation of Catalase Activity by PPAR γ Is Affected by α-Synuclein. *Ann Clin Transl Neurol* **2014**, *1*, 145–159, doi:10.1002/ACN3.38.